

# Transition to hyperbolic hyperchaos in a nonautonomous time-delay system

Pavel V. Kuptsov<sup>a,\*</sup>, Sergey P. Kuznetsov<sup>b</sup>

<sup>a</sup>*Institute of electronics and mechanical engineering, Yuri Gagarin State Technical University of Saratov, Politekhnicheskaya 77, Saratov 410054, Russia*

<sup>b</sup>*Kotel'nikov's Institute of Radio-Engineering and Electronics of RAS, Saratov Branch, Zelenaya 38, Saratov 410019, Russia*

---

## Abstract

We consider a time delay system whose excitation parameter is periodically modulated. Each new stage of excitation is seeded from the stage before the last, and due to the nonlinearity the seeding arrives with the doubled phase. As a result, the system operates as two coupled hyperbolic chaotic subsystems. Varying the relation between delay time and excitation period we affect the coupling strength between these subsystems as well as the intensity of phase doubling mechanism responsible for the hyperbolicity. Due to this the transition from non-hyperbolic to hyperbolic hyperchaos occurs. The following parts of transition scenario are revealed and analyzed: (a) intermittency as alternation of staying near a fixed point and chaotic bursts; (b) wandering between the fixed point and chaotic subset, which appears near it; (c) plain hyperchaos without hyperbolicity after termination of the visits to the fixed point; (d) transformation of hyperchaos to hyperbolic form.

*Keywords:* hyperbolic hyperchaos, finite time Lyapunov exponents, anomalous diffusion of Lyapunov exponents, embedded subsets

---

## 1. Introduction

Attractors characterized by two or more positive Lyapunov exponents are called hyperchaotic. The simplest way to obtain such an attractor is to take several chaotic, say Lorenz, systems and introduce a coupling. At small coupling strength the overall attractor will be mere a direct sum of partial attractors, and the number of positive Lyapunov exponents will be equal to the number of coupled systems [1]. However the phase space dimension in this case will be superfluous. The smallest dimension for a chaotic flow system is three so that created in this way hyperchaotic attractor with two positive Lyapunov exponents will sit in at least six-dimensional phase space. However the smallest possible dimension is four: two expanding directions, one contracting and one neutral. The first nontrivial hyperchaotic attractor in a four-dimensional system was proposed by Rössler [2].

Systems with hyperchaotic dynamics have more expanding directions in phase space so that their dynamics is expected to be more complicated in comparison with mere chaotic systems. In particular the prediction time of hyperchaotic regimes is much less than that for chaos [3]. Thus, hyperchaotic oscillators are employed when the complexity of a signal is crucial, for example for secure communications [4–7] and for image encryption [8–11]. One more promising application of hyperchaotic systems is damage assessment based on using a steady-state chaotic excitation [12].

Developing applications of chaos and hyperchaos one have to bear in mind that good scholastic properties are guaranteed only for so called hyperbolic attractors while the complexity of non-hyperbolic ones suffer because of presence of embedded stable periodic orbits [13].

---

\*Corresponding author

*Email addresses:* p.kuptsov@rambler.ru (Pavel V. Kuptsov), spkuz@yandex.ru (Sergey P. Kuznetsov)

Hyperbolic chaos plays a special role among other types of chaotic dynamics. Systems of this type, like, for example, the Smale-Williams solenoid, manifest deterministic chaos justified in rigorous mathematical sense. They demonstrate strong and structurally stable stochastic properties. They are insensitive to variation of functions and parameters in the dynamical equations, to noises, interferences etc. Moreover, hyperbolic chaotic dynamics in such systems allow a detailed mathematical analysis [13].

Hyperbolic theory [14–16] studies invariant sets in phase space of dynamical systems, including those with chaotic dynamics, composed exclusively of saddle trajectories. For all points on such a trajectory, in the space of small perturbations (tangent space), one can define a subspace of vectors, which exponentially decrease in norm under the forward time evolution, and a subspace of vectors, which exponentially decrease under the backward time evolution. In autonomous flow systems, in addition, there is a one-dimensional neutral subspace of perturbations along a trajectory that neither increase nor decrease on average. In the phase space these subspaces of small perturbations are tangent to the corresponding manifolds: A set of states that approach a given trajectory during time evolution is called the contracting (or stable) manifold of this trajectory. Similarly, the expanding (unstable) manifold is a set of states tending to the reference trajectory under the backward time evolution. Finally, the neutral manifold is related to marginally stable shifts in time. Hyperbolicity requires the absence of tangencies between stable, unstable and neutral, if any, manifolds; only intersections at nonzero angles are admitted.

Due to their great potential importance for applications, structurally stable chaotic systems with hyperbolic attractors obviously have to be a subject of priority interest, like rough systems with regular dynamics in the classic theory of oscillations [17, 18]. However, for many years the hyperbolic attractors were commonly regarded only as purified abstract mathematical images of chaos rather than something intrinsic to real world systems. A certain progress in this field has been achieved recently when many examples of physically realizable systems with hyperbolic attractor have been purposefully constructed [13, 19].

Interplay between hyperbolicity and hyperchaos was studied in Refs. [20, 21]. Paper [20] reports the scenario of transition to hyperchaos in a one-dimensional spatially distributed medium with local hyperbolic chaos. When its length is small (it corresponds to a strong coupling between local elements) all spatial elements oscillate synchronously and demonstrate hyperbolic chaos. As the length grows (the coupling strength decreases) the second Lyapunov exponent becomes positive, and spatial homogeneity is destroyed. But the hyperbolicity survives so that the system demonstrates a hyperbolic hyperchaos. Further growth of the length (or, in the other words, decrease of spatial coupling) results in the emergence of the third positive Lyapunov exponent accompanied by violation of the hyperbolicity. Paper [21] considers the violation of the hyperbolicity in a chain of diffusively coupled oscillators with hyperbolic chaos. It was shown that the violation of hyperbolicity and transition to hyperchaos occurs via an intermittency and a so called unstable dimension variability (UDV). This regime is characterized by coexistence in the chaotic attractor of invariant periodic or chaotic orbits with a different number of unstable directions [22, 23]. Since trajectories of the system can pass close to these orbits, the dimensions of their unstable and stable manifolds vary.

The UDV and intermittency as a part of scenario of transition to hyperchaos were reported in Refs. [24–26]. It is shown that the transition from chaos to hyperchaos occurs via a bifurcation similar to a blowout bifurcation [24]. In a neighborhood of the transition point one observes coexistence of unstable periodic orbits with different numbers of unstable eigenvalues. This is responsible for occurrence of UDV [25]. Moreover the transition is accompanied by so called bubbling and on-off intermittency previously observed for the attractors located at a certain invariant manifold [26].

Systems with time-delay feedback combine relative simplicity of implementation, almost like low-dimensional systems modeled by ordinary differential equations, and rich complexity of dynamics, comparable with infinite-dimensional systems associated with partial differential equations. Examples of such systems are wide-spread in electronics, laser physics, acoustics and other fields [27]. Recently several examples were suggested as realizable devices for generation of rough hyperbolic chaos [28–33]. Though rigorous mathematical proof of their hyperbolicity is not performed yet, in Refs. [34, 35] a method for numerical confirmation of the hyperbolicity based on the method of angles [36] is developed, and using this method the hyperbolicity of these systems is confirmed.

Our study in the present paper will be focused on a nonautonomous time-delay system with hyperbolic attractor suggested in Ref. [28]. Numerical confirmation of the hyperbolicity of the chaotic attractor is

performed in Ref. [34]. As discussed in paper [37], varying parameters of the system one can also obtain hyperbolic hyperchaotic attractors with as many positive Lyapunov exponents as required. In this paper we study the hyperchaotic attractor with two positive Lyapunov exponents. We perform a numerical test that confirms its hyperbolicity and analyze the details of transition from nonhyperbolic to hyperbolic hyperchaotic regime. The following scenario details are revealed. Transition from regular to hyperchaos regime occurs almost immediately - the range where only one Lyapunov exponent is positive is very narrow. Varying a control parameter we observe intermittency, UDV related anomalous diffusion of Lyapunov exponents, non-hyperbolic hyperchaos and, finally, hyperbolic hyperchaos.

The paper is organized as follows. In Sec. 2 we introduce the system and discuss how does it operate. Also we briefly review the analysis methods applied. Section 3 discusses the transition from non-hyperbolic to hyperbolic hyperchaos. It is divided in several subsections: Subsec. 3.1 is focused on Lyapunov exponents, angle between expanding and contracting subspaces, and the Kaplan-Yorke dimensions; Subsec. 3.2 represents two-dimensional distributions of various characteristic values on the attractor; in Subsec. 3.3 we deal with low dimensional subsets embedded in the attractor; and Subsec. 3.4 discusses the large time-scale behavior of finite time Lyapunov exponents (FTLEs). In Sec. 4 we outline the obtained results.

## 2. The system and methods of analysis

We will consider a nonautonomous system based on the van der Pol oscillator of natural frequency  $\omega_0$  supplied with a specially designed time-delay feedback [28]:

$$\ddot{x} - [A \cos(2\pi t/T) - x^2]\dot{x} + \omega_0^2 x = \epsilon x(t - \tau)\dot{x}(t - \tau) \cos \omega_0 t. \quad (1)$$

The parameter controlling the oscillator excitation is modulated with period  $T$  and amplitude  $A$ . Accordingly, the oscillator alternately manifests activation and damping, see Fig. 1. If the retarding time  $\tau$  is close to  $T/2$ , as shown in Fig. 1(a), the emergence of self-oscillations at each next stage of activity is stimulated by a signal emitted at the previous activity stage. Since the delayed signal is squared and mixed with auxiliary oscillations of frequency  $\omega_0$ , the stimulating force has again frequency  $\omega_0$ , but the doubled phase in comparison with the original oscillations. As a result, we get a sequence of oscillation trains with phases at successive excitation stages obeying a chaotic Bernoulli-type map,

$$\phi_n = 2\phi_{n-1} + \text{const} \pmod{2\pi}. \quad (2)$$

According to argumentation in Ref. [28], this means that the attractor for the Poincaré map, that corresponds to states obtained stroboscopically at  $t_n = nT$ , is a Smale-Williams solenoid, and the respective chaotic dynamics is hyperbolic with the first Lyapunov exponent close to  $\log 2$ . In Ref. [34] this argumentation is confirmed via numerical test for  $\tau$  values between approximately  $T/4$  and  $3T/4$ .

As reported in the paper [37], using longer retarding times, say  $\tau = 3T/2$  that provides the seeding of a new excitation stage from the stage before the previous one, see Fig. 1(b), it is possible to observe hyperchaos with two positive Lyapunov exponents. In this case the map for phases at successive excitation stages looks as follows:

$$\phi_n = 2\phi_{n-2} + \text{const} \pmod{2\pi}. \quad (3)$$

The sequence of phases now contains two independent chaotic sequences whose elements alternate. Thus, the system (1) in this case can be treated as consisting of two weakly coupled hyperbolic chaotic subsystems whose interaction produces hyperchaotic hyperbolic attractor. The subsystems interact on the boundary between excitations stages see the arc arrows in Fig. 1(b), and the hyperbolicity mechanism brings here the seeding with a doubled phase, see the polyline arrows. The type of dynamics depends on a relation between amplitudes of these two channels. This can be controlled by varying  $\tau$  or  $T$ . If  $\tau = 3T/2$ , as in Fig. 1(b), the hyperbolicity mechanism has the highest amplitude and thus dominates the coupling. In this case the subsystems operate almost independently producing the hyperbolic hyperchaos. If  $\tau \approx T$ , the hyperbolicity channel is the weakest, so that the coupling becomes more essential. In what follows, decreasing  $T$  we will observe the transition to hyperbolic hyperchaos as a result of the decrease of relative coupling strength.

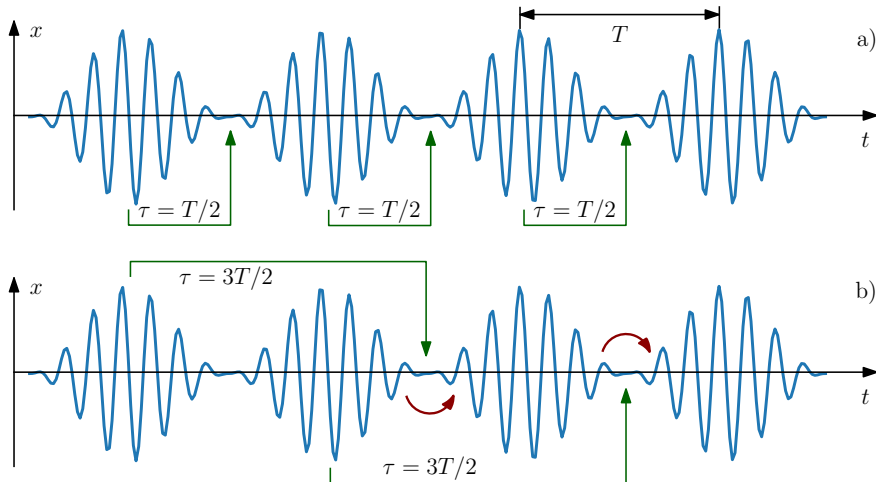


Figure 1: Operation of the system (1). (a) Hyperbolic chaos, (b) hyperbolic hyperchaos with two positive Lyapunov exponents. Polyline arrows shows the seeding transfer between excitation stages, and arc arrows show how the interaction between the subsystems occurs.

In general, for

$$\tau = (k - 1/2)T, \quad k = 1, 2, 3, \dots, \quad (4)$$

the system (1) may be expected to have a hyperchaotic attractor with  $k$  positive Lyapunov exponents  $k^{-1} \log 2$  [37].

In this paper we will focus on the case  $k = 2$  for

$$\tau = 12, \quad A = 3, \quad \epsilon = 0.3, \quad \omega_0 = 2\pi. \quad (5)$$

For sufficiently large modulation period  $T = 10$  dynamics of Eq. (1) is regular. When  $T$  gets smaller, hyperchaotic attractor appears, then it undergoes certain transformations, and finally becomes hyperbolic. At  $T = 8$  the condition (4) is fulfilled exactly.

Due to presence of the delay, the system (1) is infinite-dimensional. Dealing with its computational model, we introduce discretization along the time variable so that the dimension of the resulting model depends on the number of steps on the delay interval. For example, setting the step size  $\Delta t = 0.01$  and taking the retarding time  $\tau = 12$  we obtain for the second order delay differential equation (1) a numerical model whose phase space dimension is  $N = 2402$ .

We will analyze the system (1) numerically using Lyapunov analysis. In brief, it includes studying of expanding and contracting properties of perturbation vectors and volumes spanned by these vectors as the system runs along a trajectory. The perturbation vectors are assumed to be infinitely small in magnitude and form a linear tangent space. The dimension of this space is equal to the phase space dimension  $N$ .

Globally, i.e., for an infinitely long trajectory, properties of the tangent vectors are described by a set of Lyapunov exponents  $\lambda_i$ ,  $i = 1, 2, \dots, N$ , sorted in descending order. They can be treated in two ways. On one hand, the sum of the first  $k$  Lyapunov exponents is an average rate of exponential expansion (or contraction, if negative) of every typical  $k$ -dimensional volume in the tangent space. On the other hand, the  $n$ th Lyapunov exponent is an average rate of exponential expansion of the  $n$ th covariant Lyapunov vector (CLV). These vectors are named ‘‘covariant’’ since  $n$ th vector at time  $t_1$  is mapped by a tangent flow to the  $n$ th vector at time  $t_2$  for any  $t_1$  and  $t_2$ . There is a unique set of  $N$  such vectors. An arbitrary tangent vector does not have this property and merely converges to the first CLV. Two algorithms for computation of CLVs were first reported in the pioneering works [38, 39]. See also paper [40] for more detailed explanation and discussion of one more algorithm. Also see book [41] for a survey.

Using the Lyapunov exponents one can compute Kaplan-Yorke dimension of the attractor [42].

$$D_{KY} = m + \frac{\sum_{i=1}^m \lambda_i}{|\lambda_{m+1}|}, \quad (6)$$

where  $m$  is such that  $\sum_{i=1}^m \lambda_i > 0$  and  $\sum_{i=1}^{m+1} \lambda_i < 0$ . The Kaplan-Yorke dimension is related with the information dimension and is an upper estimate for the Hausdorff dimension of an attractor [43].

Local structure of the attractor can be analyzed using finite time Lyapunov exponents (FTLEs)  $\ell_i$ . There are two different sorts of these exponents. One is obtained in the course of the standard algorithm for Lyapunov exponents when we iterate a set of tangent vectors and periodically orthonormalize them using Gram-Schmidt or QR algorithms. Logarithms of their norms divided by the time step between the orthonormalizations may be called Gram-Schmidt FTLEs. This sort of FTLEs characterizes local volume expanding properties in the tangent space. The sum of the first  $k$  Gram-Schmidt FTLEs is a rate of local exponential expansion of a typical  $k$ -dimensional tangent volume. Their individual values except the first one have no much sense. Another sort of FTLEs are computed as local exponential expansion rates for CLVs. They characterize expansion or contraction for individual vectors in tangent space. In more detail, the difference between these two sorts of FTLEs is discussed in Ref. [44]. In what follows we will consider the CLV based FTLEs.

Dealing with FTLEs for flow systems, one have to choose an appropriate time step. This is not so obvious since the choice must be related somehow with intrinsic attractor time scales, which are usually a priori unknown. One way to put the FTLEs analysis on the solid ground is to consider them on infinitesimally small times. Such instant FTLEs were introduced in paper [44].

The instant FTLEs make sense for flow systems while for discrete time systems instead of them one can consider one step FTLEs. Since the system under consideration in this paper operates under external forcing with period  $T$ , it is natural to consider the corresponding stroboscopic map for it. Thus all FTLEs below will be computed for one step of this map, i.e. for one period  $T$  in terms of the original flow system.

Another way of using FTLEs is to consider them on asymptotically long times. For large time scale the Gram-Schmidt and the CLV based FTLEs coincide [40], so it is reasonable to consider the Gram-Schmidt ones since their computations is much less time consuming. Due to the decay of correlations for a typical chaotic processes on large time scales, pairwise covariances of Lyapunov sums  $L_i$  (FTLEs not divided by time step) are expected to grow linearly. The matrix  $D_{ij}$  of rates of linear growth of covariance of Lyapunov sums  $L_i$  and  $L_j$  is introduced and studied in Ref. [45]. In this paper we will analyze covariances of the Lyapunov sums and show that for some parameter values the covariances obey power law instead of the expected linear one.

To characterize the hyperbolicity we will use the angle criterion. Chaotic attractor is called hyperbolic when all its trajectories are of saddle type. It means that its expanding and contracting manifolds never have tangencies. Verification of this property can be done by checking the angles between tangent subspaces spanned by CLVs corresponding to positive and negative Lyapunov exponents (or, more rigorously, the smallest principal angle between the subspaces). The angle  $\theta_i$  is the angle between a subspace spanned by the first  $i$  CLV and the subspace spanned by all the rest of them. If a discrete time system has  $k$  positive Lyapunov exponents and all others are negative then it will be hyperbolic if  $\theta_k$  never vanish along trajectories on the attractor. As we consider a system with two positive Lyapunov exponents, the indicating angle is  $\theta_2$ . Notice that in actual computations starting from random initial conditions we will never get exact zero angle. Instead, a typical trajectory can pass arbitrary close to points with zero angles. Thus verifying the hyperbolicity we can only check if the angles get very small. The fast method of computation of the angles is developed in papers [36, 40], and its implementation for time delay systems can be found in Refs. [34, 35].

A chaotic attractor is known to contain embedded invariant subsets, in particular, periodic orbits, and there are effective numerical methods for detection these embedded orbits [46–48]. Nevertheless, application of these methods for high-dimensional systems is rather problematic yet. In this paper we use another approach to analyze the embedded subsets. The idea is as follows. Assume that running along a trajectory we encounter a point where some of CLVs merge, i.e., the angles between them vanish. This degeneracy is possible when the point belongs to a subset whose embedding dimension is lower then the dimension of the

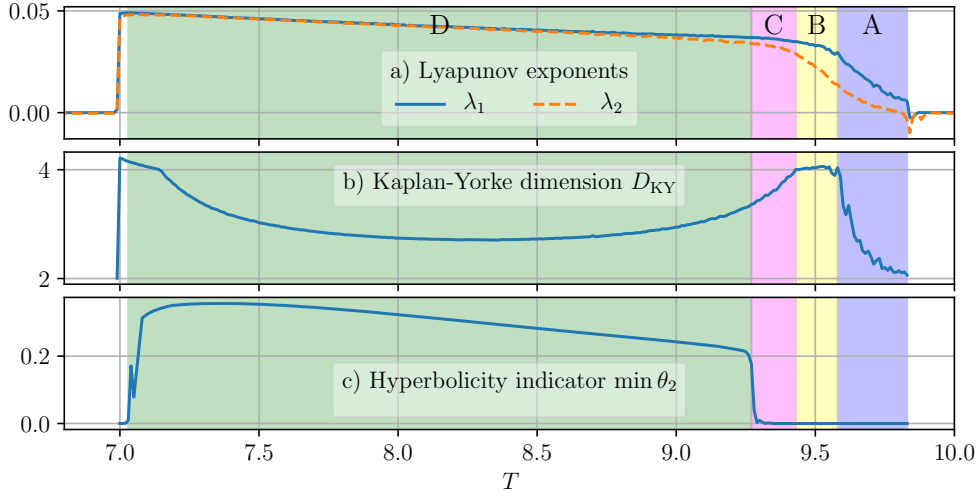


Figure 2: (a) Lyapunov exponents, (b) Kaplan-Yorke dimension and (c) Minimal angle  $\theta_2$  between expanding and contracting tangent subspaces. Shaded areas A, B, C and D highlight ranges of different attractor types.

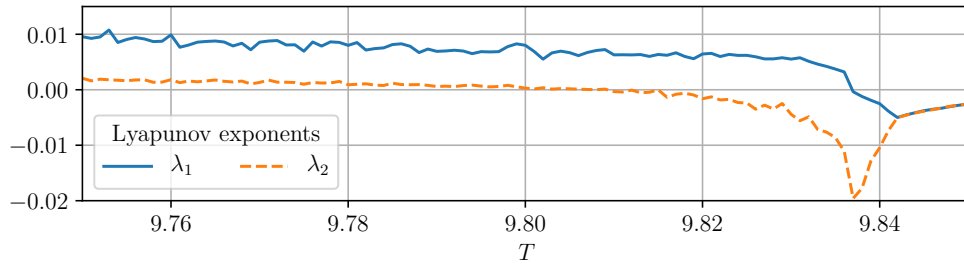


Figure 3: Enlarged area of Fig. 2(a) where the transition from chaos to hyperchaos occurs.

whole phase space. This subset can be identified by indexes of merging CLVs. We will compute the CLV based FTLEs for each such subset separately and plot them against the control parameter, thus observing how the embedded subsets are transformed. Notice that this approach has the following limitations: it detects only lower-dimensional subsets and ignores those whose embedding dimension coincides with the dimension of the attractor; also it cannot distinguish different subsets with identical signatures. Nevertheless, as we will see below, this method can give appropriate and valuable information about the structure of the attractors.

Since we analyze a high-dimensional system, visualizing of the attractors is a non-trivial question. Preferably, we will consider simple projection of the attractors onto the plane  $x$  and  $\dot{x}$ . But to reveal more information about their structure we will also consider so-called Isomap projections. This is a content of a nonlinear dimension reduction method employed in data science to eliminate non-essential features from high-dimensional data sets [49].

### 3. The analysis

#### 3.1. Lyapunov exponents, Kaplan-Yorke dimension and angles between tangent subspaces

First, for the system (1) with parameters (5) we consider minimal angle, two Lyapunov exponents and Kaplan-Yorke dimension as functions of  $T$  decreasing from 10 to 7, see Fig. 2. Near  $T = 10$  there are no positive Lyapunov exponents, as one can see in Fig. 2(a). It corresponds to regular oscillations in the system.



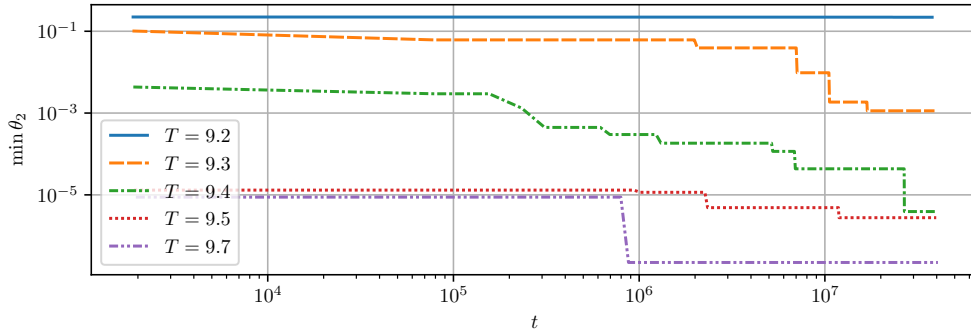


Figure 4: Minimal angle  $\theta_2$  as a function of time  $t$ . Log-log plot is used. Curve  $T = 9.2$  corresponds to hyperbolic chaos, and curves with  $T \geq 9.3$  reveal non-hyperbolic attractors.

Transition to chaos and then to hyperchaos is illustrated in Fig. 3 where the enlarged area of Fig. 2(a) is shown. One can see that the dynamics becomes chaotic at approximately  $T = 9.835$ . There is a very narrow area where only one Lyapunov exponent exists, and very soon approximately at  $T = 9.8$  the second one also becomes positive, so the hyperchaotic regime appears. Observe very small slope of the curve  $\lambda_2$ : It goes almost horizontally when passes zero. This is typical behavior for transition to hyperchaos owing to the bifurcations of unstable periodic orbits embedded into attractor [25]. In our case the area where  $\lambda_2$  stays close to zero is very narrow.

Parameter interval of our interest can be split into four areas that we mark by capital letters A, B, C, and D, see Fig. 2. Area A starts when the system becomes hyperchaotic at  $T = 9.8$  and extends to  $T = 9.58$  until the Kaplan-Yorke dimension grows, see Fig. 2(b). Within this area the first two Lyapunov exponents grow almost linearly with similar slopes, see Fig. 2(a). The minimal angle  $\min \theta_2$  between the expanding and contracting subspaces remains close to zero Fig. 2(c) indicating non-hyperbolicity of chaos within this area.

Area B covers the range where the Kaplan-Yorke dimension is constant and ends at approximately  $T = 9.43$ , see Fig. 2(b). Here the second Lyapunov exponent continues to grow while the first one approaches the saturation, Fig. 2(a). The minimal angle  $\min \theta_2$  is still zero, i.e. chaos is non-hyperbolic.

Area C stretches up to a point of transition to hyperbolic chaos, i.e., to a point where the minimal angle  $\theta_2$  starts to grow. It occurs at approximately  $T = 9.27$ .

Area D corresponds to hyperbolic hyperchaos with two positive Lyapunov exponents. In this area two first Lyapunov exponents approach each other and almost merge. The transition to a hyperbolic attractor occurs smoothly: no visible features on the boundary between areas C and D can be seen in the curves for Lyapunov exponents and Kaplan-Yorke dimension, see Fig. 2(a) and (b). This area ends at approximately  $T = 7.02$ . Beyond this point the system remains hyperchaotic within the very narrow interval and then oscillations become regular.

As already mentioned, a typical trajectory on a non-hyperbolic attractor started from random initial conditions does not contain points with exactly zero angle  $\theta_2$ . However the trajectory can pass near such points arbitrary close so that  $\theta_2$  can be arbitrary small. On the contrary, for trajectories on a hyperbolic attractor the angle  $\theta_2$  is well separated from zero. Thus, to perform one more test of the hyperbolicity we can consider a function  $\min \theta_2(t)$ , where the minimum is computed on the interval  $[0, t]$ . For non-hyperbolic attractors this function decays, while for hyperbolic ones it must saturate at some level. This function for different  $T$  is shown in Fig. 4. Behavior of the curve at  $T = 9.2$  indicates the hyperbolicity since the function does not decay, and the decaying functions at  $T \geq 9.3$  reveal non-hyperbolicity.

### 3.2. Probability density functions on the attractor

To examine the attractor structure in areas A, B, C and D we will consider now probability density functions (PDFs) of dynamical variables and related characteristic values, see Fig. 5. Plots in this figure

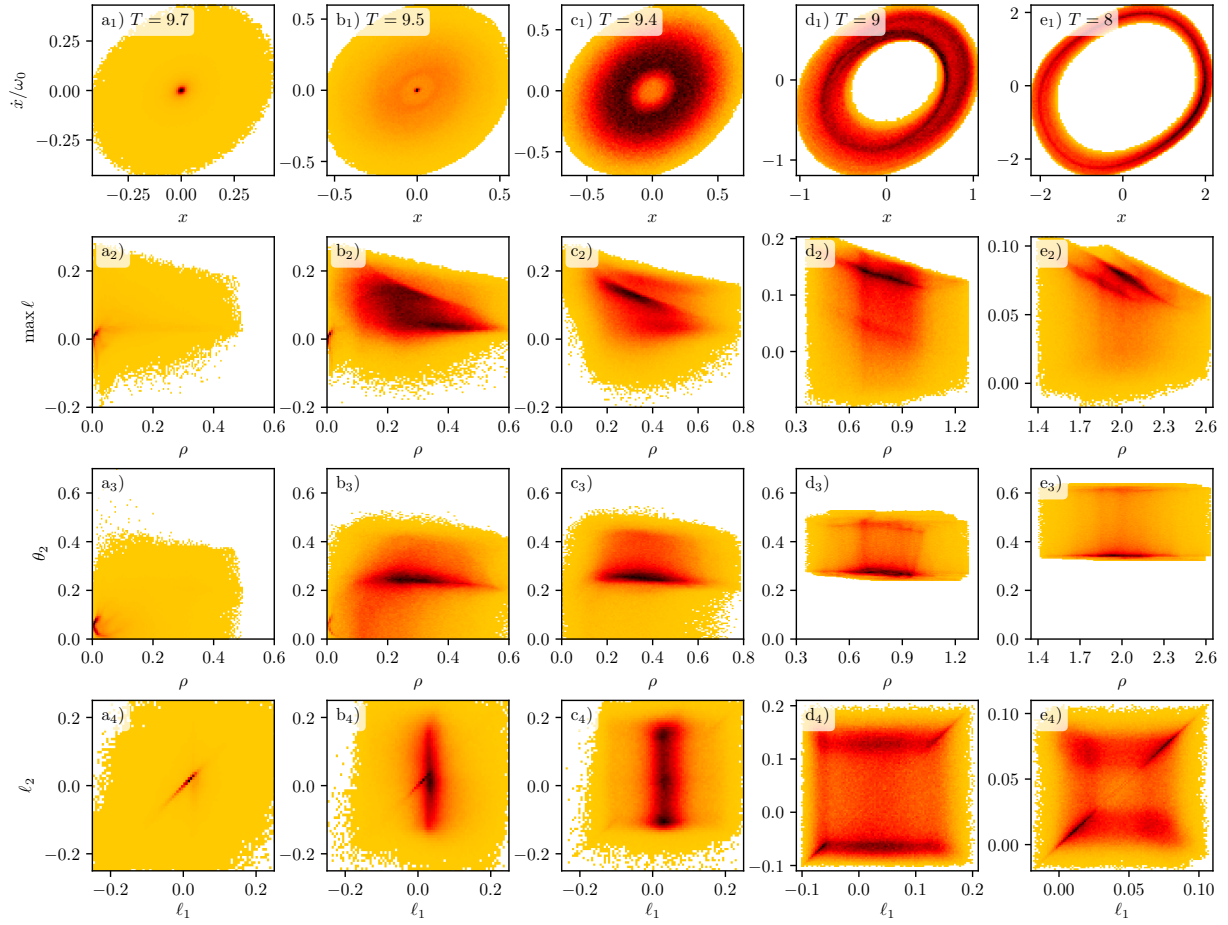


Figure 5: Numerical approximations of probability density functions (2D histograms) on the attractor. Columns (a), (b), and (c) correspond to areas A, B, and C in Fig. 2, respectively, and columns (d) and (e) correspond to the area D. Values of  $T$  are given in the legends on the top row and are the same along the columns. Values on the vertical axis in the leftmost column are the same along rows. Darker areas represent higher densities.



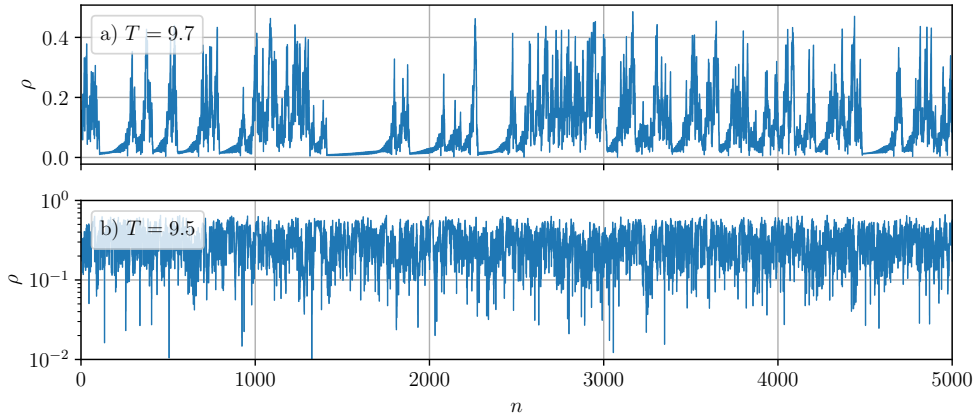


Figure 6: Time series of distances to the origin for (a)  $T = 9.7$ , area A, (b)  $T = 9.5$ , area B.

are grouped in five columns. The first three of them, from (a) to (c), correspond to the areas from A to C in Fig. 2, and two last columns (d) and (e) represent the area D. Column (d) characterizes a hyperchaotic hyperbolic attractor close to the transition point and (e) corresponds to the case when the relation (4) is fulfilled exactly for  $k = 2$ , i.e.,  $\tau = 1.5T$ . All plots are computed for the stroboscopic map at  $t = nT$ .

### 3.2.1. Area A

Figures 5(a<sub>1,2,3,4</sub>) are plotted at  $T = 9.7$  that corresponds to the area A. Panel (a<sub>1</sub>) shows PDF of  $x$  and  $\dot{x}/\omega_0$ . Since the phase space dimension is high, these plots can be considered as two-dimensional projections of multidimensional PDFs. Observe a sharp spike at the origin visible as a dark spot. The spot is surrounded by a wide pale area representing wandering of the system in the vicinity of the origin.

The observed structure of PDF is caused by intermittency, see Fig. 6(a). In this figure we plot the phase space distance of the orbit to the origin

$$\rho(t) = \sqrt{x(t)^2 + (\dot{x}(t)/\omega_0)^2} \quad (7)$$

for time sliced stroboscopically at  $t = nT$ . One can see alternation of laminar phases when the system is close to zero with burst of oscillations. Figure 7 provides further confirmation of the intermittent nature of the considered regime. It shows a distribution of lengths of laminar trajectory cuts when the phase space trajectory is near the origin<sup>1</sup> In the log-log scale the distribution admits linear approximation that corresponds to the power law. The computed exponent is  $\alpha = -1.95$ .

Figure 5(a<sub>2</sub>) shows PDF of  $\rho$  and maximal FTLE  $\max \ell_i$ ,  $i = 1, 2, \dots$ . Here and below FTLEs  $\ell_i$  are computed as average exponential growth rates of CLVs over time  $T$ , corresponding to one step of the stroboscopic map. Since FTLEs strongly fluctuate, they are usually not ordered in the descent order in contrast to the global Lyapunov exponents. Hence, on each step we simply take the largest one.

The PDF of  $\rho$  and  $\max \ell$  in Fig. 5(a<sub>2</sub>) shows locations of areas of chaotic divergence on the attractor and areas where close trajectory approach each other. One can see a spike at  $\rho = \max \ell = 0$ . It corresponds to the laminar phases and indicates that close to the phase space origin  $\rho = 0$  the trajectories basically demonstrate marginal stability. To explain this, we need to take into account that  $x = \dot{x} = 0$  is a fixed point for the considered system (1). Linearization near this point results in a linear equation with parametric excitation with the period  $T$ . Since the excitation parameter oscillates symmetrically near zero, on average the fixed point at the origin is marginally stable.

<sup>1</sup>Here and below power law distributions as well as estimation of the exponent  $\alpha$  is done with the help of Python package “powerlaw” [50].

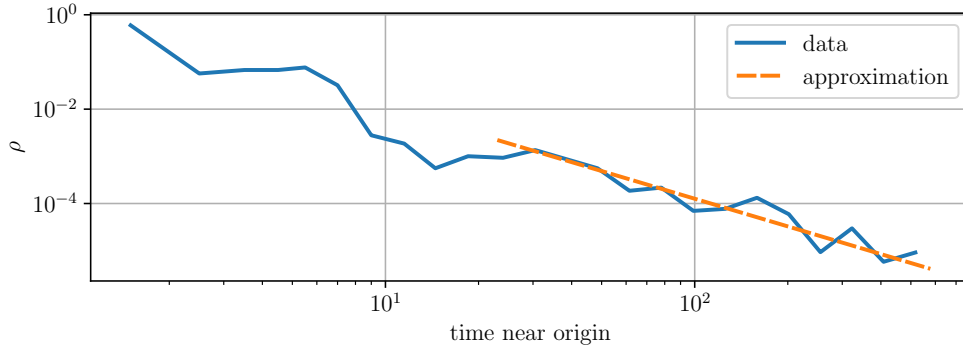


Figure 7: Distribution of laminar phases  $\rho < 0.05$  and its power law approximation with the exponent  $\alpha = 1.95$  that corresponds to Figs. 5(a) and 6(a), area A.

Figure 5(a<sub>3</sub>) shows PDF of  $\rho$  and the angle  $\theta_2$  whose zero indicates a tangency between expanding and contracting manifolds, i.e., reveals points of the hyperbolicity violation. From Fig. 2(c) we know that within the area A chaos is non-hyperbolic. And from Fig. 5(a<sub>3</sub>) we see that the violation of the hyperbolicity preferably occurs near the origin: one can see the spike near  $\rho = 0$  where  $\theta_2$  often vanishes. Beyond the origin the vanishing angles are more rare.

Figure 5(a<sub>4</sub>) represents PDF of two first FTLEs  $\ell_1$  and  $\ell_2$ . The dark line along the diagonal near the origin corresponds to equal  $\ell_1$  and  $\ell_2$ . Identical Lyapunov exponents reflect a symmetry of dynamics with respect to some variables interchange. As discussed above, see Fig. 1, within the considered parameter range the system can be treated as two weakly coupled chaotic subsystems. The stripe along the diagonal in Fig. 5(a<sub>4</sub>) indicates that these two subsystem behave coherently, i.e., synchronized, when pass the origin.

### 3.2.2. Area B

PDF of  $x$  and  $\dot{x}/\omega_0$  in the area B, see Fig. 5(b<sub>1</sub>), looks very similar to the previous case in Fig. 5(a<sub>1</sub>). The only difference is a barely visible darker area surrounding the origin. But this results in a qualitative change of the behavior. One can see in Fig. 6(b) that though the trajectory still often visits the origin neighborhoods, this is not an intermittency.

PDF of  $\rho$  and  $\max \ell$  in Fig. 5(b<sub>2</sub>) reveals the emergence in the area B of a new structure. Like in the area A, see Fig. 5(a<sub>2</sub>), we observe the spike at  $\rho = \max \ell = 0$  corresponding to the passing of a trajectory near the fixed point at the origin. But also a massive bulk of points appears at positive  $\max \ell$  and nonzero  $\rho$ . It represents a chaotic subset embedded into the attractor. Thus in the area B the dynamics is determined by a wandering of a system between this chaotic subset and the fixed point at the origin.

PDF of  $\rho$  and  $\theta_2$  in Fig. 5(b<sub>3</sub>) again, similarly to the area A, see Fig. 5(a<sub>3</sub>), contains the spike near  $\rho = \theta_2 = 0$  (now barely visible due to the presence of another maxima) but also a large spot corresponding to a new chaotic subset. Most of points within this spot are hyperbolic, i.e., located at  $\theta_2 > 0.2$ . However, their noticeable number is characterized by a vanishing angle: observe getting down to  $\theta_2 = 0$  darker arm centered at approximately  $\rho = 0.2$ .

PDF of  $\ell_1$  and  $\ell_2$ , see Fig. 5(b<sub>4</sub>), again contains the diagonal line near zero mentioned already in the area A in Fig. 5(a<sub>4</sub>) and corresponding to the coherence of the subsystems near the origin. Also a very well pronounced is the vertical stripe representing strong fluctuation of the second FTLE  $\ell_2$ . The first one  $\ell_1$ , on contrary, is well localized.

Altogether, in the area B a new embedded non-hyperbolic chaotic subset emerges but the fixed point at the origin is essential yet and trajectories wander between these two subsets. Due to this wandering, the FTLEs  $\ell_1$  and  $\ell_2$  switch between coherency at the origin and strong fluctuation of  $\ell_2$  at the chaotic subset. As shown below, the presence of two competing embedded subsets results in anomalous diffusion of Lyapunov exponents.

### 3.2.3. Area C

Figure 5(c<sub>1</sub>) corresponds to the area C. One can see that darker and barely visible circular structure in Fig. 5(b<sub>1</sub>) is now turned into a well formed ring where trajectories spend most of time. There is no maximum corresponding to the fixed point at the origin anymore, but its neighborhood is still visited.

In Fig. 5(c<sub>2</sub>) we observe that the spike at  $\rho = \max \ell = 0$  disappears at all, and the origin  $\rho = 0$  is characterized by a positive FTLE. Thus, the chaotic subset first appeared in Fig. 5(b<sub>2</sub>) now dominates. Representing its structure on the PDF becomes sharper in comparison with Fig. 5(b<sub>2</sub>): one can see well defined dark stripe on the plot indicating that the most probable largest FTLEs decrease as  $\rho$  grows.

Figure 5(c<sub>3</sub>) also confirms disappearance of the structure representing the fixed point at the origin. The dominating chaotic subset becomes “more hyperbolic” insofar as the getting down arm near  $\rho = 0.2$  disappears and less number of points has the vanishing angle  $\theta_2$ .

In accordance with the changed role of the fixed point, in Fig. 5(c<sub>4</sub>) no diagonal stripe is visible representing the coherence of  $\ell_1$  and  $\ell_2$  at the origin. The only most visited structure is a vertical stripe corresponding to the chaotic subset that now dominates. Moreover barely visible are two more features. The first is a pair of diagonal segments appeared beyond the origin at approximately  $\ell_1 = \ell_2 \approx \pm 0.15$ , and the second are darker areas to the left and to the right from the main vertical stripe representing a more intense fluctuations of  $\ell_1$ . These features are precursors of a hyperchaotic hyperbolic attractor that appears in the course of further decrease of  $T$ .

### 3.2.4. Area D

Figures 5(d) and (e) represent a hyperchaotic hyperbolic attractor, the area D in Fig. 2. The common feature is that trajectories never visit vicinities of the origin, see Figs. 5(d<sub>1</sub> and e<sub>1</sub>). It means that oscillation phase that is responsible for the hyperbolic chaos is now well defined [37].

Inspection of PDFs in Figs. 5(d<sub>1</sub> and e<sub>1</sub>) reveals two different forms of the attractor. At  $T = 9$ , i.e., just after the transition to the hyperbolicity, there are two loops formed by the most visited points while far from the transition at  $T = 8$ , only one main loop is visible. We recall that hyperchaos in the considered system (1) is the result of interaction of two coupled chaotic subsystems, see Fig. 1(b) and the related discussion. When  $T$  is decreased the coupling strength between the subsystems becomes weaker while the hyperbolicity mechanism, related with the phase doubling, becomes stronger. Comparing Figs. 5(d<sub>1</sub>) and (e<sub>1</sub>) we can see that it results in more coherent behavior of these subsystems that manifests itself as a merge of the two loops.

Visually the attractor in Fig. 5(d<sub>1</sub>) looks more complicated than the attractor in Fig. 5(e<sub>1</sub>) and one can expect that its dimension is higher. This intuition agrees with Fig. 5(b): the Kaplan-Yorke dimension decreases as  $T$  is varied within the area D from  $T = 9$  to  $T = 8$ .

PDF of  $\rho$  and  $\max \ell$  has a single stripe when the coupling between the chaotic subsystems is stronger at  $T = 9$ , see Fig. 5(d<sub>2</sub>) while weaker coupling at  $T = 8$  results in two parallel stripes. The latter indicates that two chaotic subsets may be distinguished, in the phase space and a trajectory wanders between them. Taking into account the discussion of Figs. 5(d<sub>1</sub> and e<sub>1</sub>) that at  $T = 8$  the two subsystems are more coherent, one can assume that these subsets correspond to synchronized and non-synchronized segments of trajectories. Unlike the case in Fig. 5(b<sub>2</sub>) these two subsets have similar properties so that, as we will discuss below, their presence does not affect the normal convergence of Lyapunov exponents. Also notice that most of points in Figs. 5(d<sub>2</sub> and e<sub>2</sub>) are located at positive values of  $\max \ell$ . It means that already locally the fluctuations of FTLEs are sufficiently weak.

Also the emergence of the two subsets at  $T = 8$  is visible in PDFs of  $\rho$  and  $\theta_2$ , see Figs. 5(d<sub>3</sub> and e<sub>3</sub>). In the panel d<sub>3</sub> we observe the main dominating structure as a dark horizontal stripe at the bottom of the plot, while in the panel (e<sub>3</sub>) one also can see one more horizontal stripe at the top part. It means that the two chaotic subsets has different distributions of angles between expanding and contracting manifolds though in both cases the angles are non-vanishing. The latter again confirms the hyperbolicity of chaos in the area D.

In PDF for  $\ell_1$  and  $\ell_2$  in Fig. 5(d<sub>4</sub>) the features barely visible in Fig. 5(c<sub>4</sub>) are well pronounced. Both of FTLEs fluctuate with almost identical amplitudes. Both positive and negative values are encountered but the fluctuations are strongly biased to the positive side. Prevailing structures are two horizontal stripes

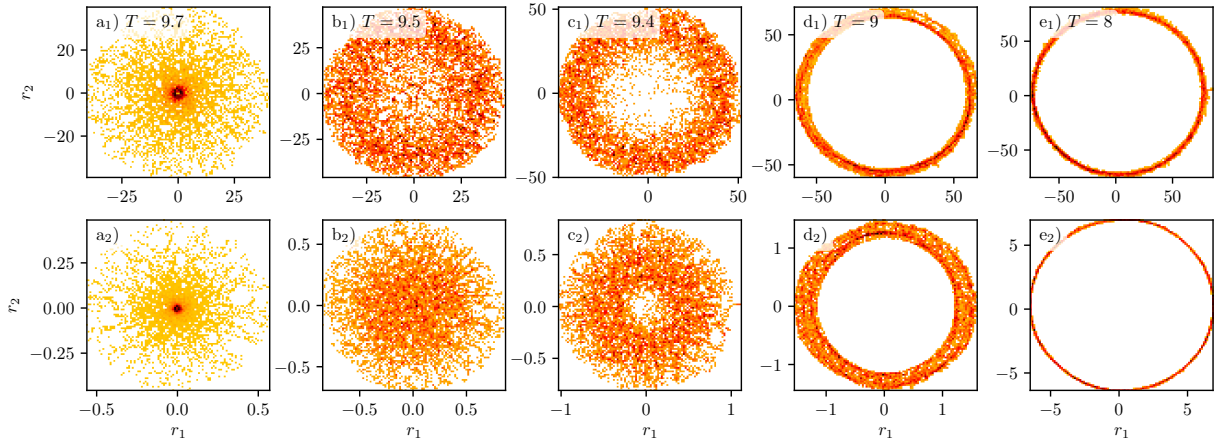


Figure 8: PDFs of Isomap projections. For the first row the isomap reduction is done for the full length state vectors, and the second row is obtained after the reduction of vectors including the first and the last points of the delay interval.  $r_1$  and  $r_2$  denote the first and second reduced components, respectively.

representing fluctuations of  $\ell_1$  and two short diagonal segments corresponding to synchronous oscillations of the two subsystems. Since the presence of the synchronized segments is revealed only in PDF of  $\ell_1$  and  $\ell_2$ , we conclude that at  $T = 9$  the coherency between the subsystems occurs but it is weak and seldom.

As  $T$  is decreased up to 8, the PDFs of  $\ell_1$  and  $\ell_2$  become symmetric with respect to the main diagonal, see Fig. 5(e<sub>4</sub>). It demonstrates presence of two identical chaotic subsystems that can oscillate coherently, see the well formed diagonal stripe. But they do not stay synchronized for all time. Ends of the coherent stages associated with leaving the symmetric attractor are represented by symmetric off-diagonal structures. Also notice that the whole area of FTLEs fluctuations is roughly four times narrower than in the previous cases and fluctuating FTLEs are preferably positive.

### 3.2.5. Isomap projections

As we already mentioned above, the dimension of the numerical state vector of the system (1) in our concrete computations is  $N = 2402$ . Projecting the multidimensional attractor onto the plane of  $x(t)$  and  $\dot{x}(t)$  we can omit a huge amount of information. On the other hand side, Eq. (1) includes only the first and the last points of the delay interval:  $x(t)$ ,  $\dot{x}(t)$ ,  $x(t - \tau)$ ,  $\dot{x}(t - \tau)$ , and we can expect that actually a multidimensional attractor belongs to the corresponding four-dimensional manifold. In order to estimate how much essential information is lost when the attractor is projected onto the plane of  $x$  and  $\dot{x}$  we compare PDFs in Figs. 5(a<sub>1</sub> - e<sub>1</sub>) with those obtained via a more sophisticated projection algorithm named Isomap. This algorithm performs a nonlinear dimension reduction employing the hypothesis that each state vector together with its nearest neighbors share the same fragment of a smooth low-dimensional manifold. Thus this manifold is found through an unfolding of a mesh of geodesic, i.e., the shortest, distances between these neighboring vectors [49].

Figures 8(a) - (e) show the isomap projections of the multidimensional attractor whose simple two-dimensional projections were presented in Figs. 5(a<sub>1</sub>) - (e<sub>1</sub>). The first row, i.e., Figs 8(a<sub>1</sub> - e<sub>1</sub>), are PDFs obtained after reduction of state vectors of full length  $N = 2402$ . For the second row, Figs. 8(a<sub>2</sub> - e<sub>2</sub>), we have reduced the four-dimensional state vector including the first and the last points of the delay intervals. First of all notice that two represented versions of isomap projections look very similar. It means that the actual dimension of the manifold where the attractor belongs is anyway not higher than four. Qualitatively isomap projections in the area A (panel (a)), are similar to the simple projection in Fig. 5(a<sub>1</sub>). It means that the latter provide adequate information about the attractor structure. The same is the case for areas C (panel (c)) and D (panels (d) and (e)).

The most notable difference is observed in the area B. Unlike simple projection in Fig. 5(b<sub>1</sub>), the isomap

projections in Figs. 8(b<sub>1</sub>) and (b<sub>2</sub>) demonstrate sufficiently uniform distributions without any more or less noticeable most visited locations. This discrepancy allow to conclude that the embedding dimension of the attractor here is higher then two. We recall that the Kaplan-Yorke dimension within this area also attains its maximum, see Fig. 2(b). The uniform distributions may be regarded as a manifestation of strong trajectory fluctuations caused by the presence in the phase space of two competing subsets, see the discussion of Fig. 5(b<sub>1</sub>) above.

### 3.3. Low-dimensional embedded subsets

When we move along a trajectory and compute CLVs  $\gamma_i$  we can register cases when some of the vectors have zero angles in between. This happens when we pass close to an invariant attractor subsets whose embedding dimension is lower than dimension of the attractor itself. All such subsets will be identified by signatures listing what vectors coincide, say  $\gamma_i = \gamma_j$ . Each subset will be characterized by partial Lyapunov exponents  $\tilde{\lambda}$  computed as average of the corresponding FTLEs.

#### 3.3.1. Partial Lyapunov exponents for the embedded low-dimensional subsets

Figure 9 represents partial Lyapunov exponents (left column) and their scaled weights (right column). We use the latter term to refer to a number  $n$  of encountered points with this signature divided by the total number of checked attractor points  $N = 10^6$  and multiplied by 100. We show only those signatures in the figure that have noticeable scaled weights. Signatures that are encountered less then 50 times for  $10^6$  checked points are omitted.

Figures 9(a) represent trajectory points without peculiarities, i.e., where no merging of CLVs was encountered. As one can see in panel (a<sub>2</sub>) their number is much higher then the number of points with merging CLVs and their scaled weight is close to the maximum. In fact, the curves shown in Fig. 9(a<sub>1</sub>) coincide with the ordinary global Lyapunov exponents, cf. Fig. 2(a).

Figures 9(b), (c) and (d) demonstrate the dominating embedded low-dimensional structures. Their signatures are  $\gamma_1 = \gamma_2$ ,  $\gamma_3 = \gamma_4$ , and  $\gamma_5 = \gamma_6$ , respectively. Their relative weights are around  $0.1 \div 0.2$ , see panels (b<sub>2</sub>), (c<sub>2</sub>), and (d<sub>2</sub>). Observe that partial Lyapunov exponents in the panels (b<sub>1</sub>), (c<sub>1</sub>), and (d<sub>1</sub>) are similar to those without merging CLVs in Fig. 9(a<sub>1</sub>). The common feature of these three cases is that partial Lyapunov exponents are either pairwise coincide or close to each other: 1 and 2, 3 and 4, 5 and 6. This is the manifestation of the presence of two chaotic subsystems, see Fig. 1(b) and the related discussion. Pairwise closeness of the partial Lyapunov exponents is related with the coherence of these subsystems, discussed above.

The scaled weight of the subset  $\gamma_2 = \gamma_3$  in Figs 9(e) is smaller in order of magnitude. However, this subset is nevertheless essential. We recall that the whole attractor has two-dimensional expanding manifold so that the vanishing angle between the second and the third CLVs indicates the destruction of the hyperbolicity. Thus Fig. 9(e<sub>1</sub>) represents the subset responsible for the violation of the hyperbolicity. Observe that it disappears in the middle of the area C, before the transition to hyperbolicity on the C-D boundary. This is explained in Fig. 9(e<sub>2</sub>). One can see that the number of the encountered points monotonically decay within the area C as  $T$  approaches the area D. The system visits the subset  $\gamma_2 = \gamma_3$  more and more seldom so that one have to trace longer and longer trajectories to observe this subset close to the transition point.

Also notice that the destructing hyperbolicity subset  $\gamma_2 = \gamma_3$  has the largest weight in the area A. This agrees well with the previous observations in Figs. 5(a<sub>3</sub> - e<sub>3</sub>): The highest maximum of PDF near  $\theta_2 = 0$  indicating the disappearance of the hyperbolicity is observed in the area of intermittency A.

The weight of the subset  $\gamma_4 = \gamma_5$  in Figs 9(f) is also relatively small. This subset becomes hyperchaotic in the area B, and two largest Lyapunov exponents become almost identical in the area D, when the system becomes hyperbolic. Since its second and third CLVs do not merge, this subset is hyperbolic. Also it is located far from the symmetric manifold where the two subsystems are synchronized since their partial Lyapunov exponents are not close pairwise as in Figs. 9(b, c, and d). It explains the existence of two forms of hyperbolic attractors that where demonstrated in Fig. 5(d) and (e): Less coherent attractor (column (d)) exists to the right of  $T \approx 8.5$  when the subset in Figs 9(f) is visited, and it becomes more coherent (column (e)) when this subset disappears.

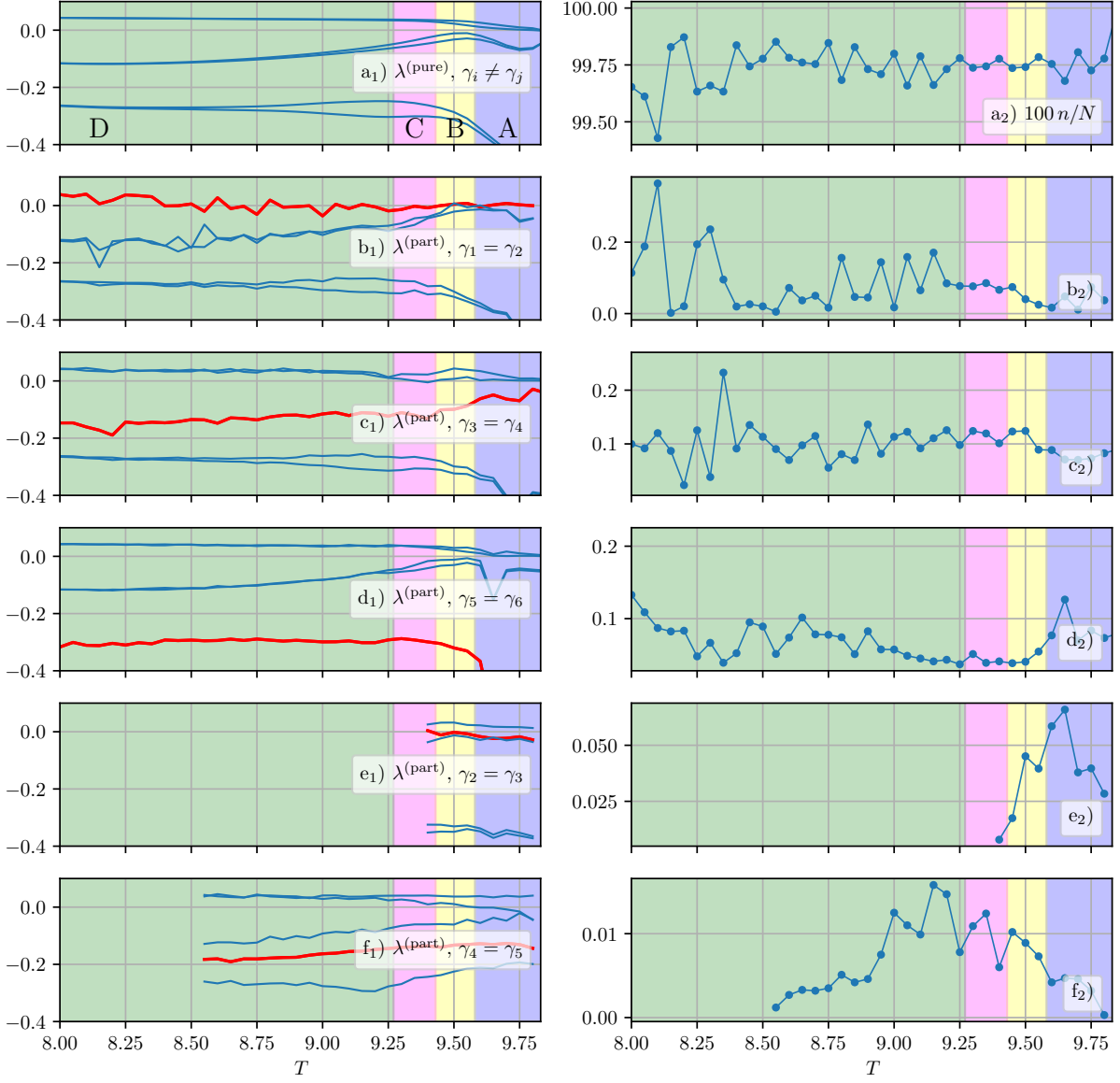


Figure 9: Embedded subsets.  $n$  means number of such points averaged along  $T$ .  $N = 10^6$ .  $\tilde{\lambda}$  is a partial Lyapunov exponents. Fat red line shows the coinciding partial Lyapunov exponents.

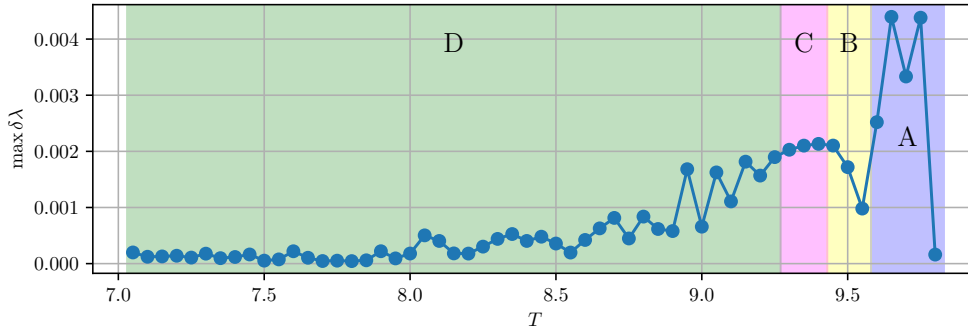


Figure 10: Maximal relative bias of Lyapunov exponents due to embedded low-dimensional subsets  $\max\{\delta\lambda_i | i = 1, 2, \dots, 6\}$ , see Eq. (8).

### 3.3.2. Bias of global Lyapunov exponents due to low-dimensional embedded subsets

Now we estimate overall influence of lower-dimensional embedded subsets. For each  $T$  we first compute the Lyapunov exponents  $\lambda_i$  as average of all CLV FTLE encountered along a trajectory. Then we compute purified Lyapunov exponents  $\lambda_i^{(\text{pure})}$  ignoring those FTLEs obtained at points near the subsets. Finally we estimate the relative bias introduced by the embedded lower-dimensional subsets as

$$\delta\lambda_i = \left| \frac{\lambda_i - \lambda_i^{(\text{pure})}}{\lambda_i} \right|. \quad (8)$$

Figure 10 shows the maximal relative bias computed for six Lyapunov exponents as  $\max\{\delta\lambda_i | i = 1, 2, \dots, 6\}$ . Observe clear difference of areas A, B, C and D. In the area A, where the system demonstrates intermittency, the bias is the highest. The area B is characterized by the presence of two competing subsets embedded into the attractor. In the beginning of this area, the bias first drops down but then grows again. In the area C, where the system has chaotic non hyperbolic attractor, the bias remains at a constant level.

In the area D, where the attractor becomes hyperbolic, we observe a decrease of the bias. It occurs until the subset  $\gamma_4 = \gamma_5$  is visited, see Figs 9(f), so that the hyperbolic attractor has the less coherent form shown in Figs. 5(d). After the disappearance of this subset, when the attractor becomes more coherent (see Figs. 5(e)) the bias stays at more or less constant small level. Small bias is a manifestation of the uniformity of the hyperbolic attractor, see Refs. [13, 19].

### 3.4. Large time FTLEs

Another approach considers fluctuations of FTLEs on large times. Unlike previously discussed FTLEs based on CLVs computed for one period of excitation  $T$ , i.e., for one step of stroboscopic map at  $t_n = nT$ , now we average FTLEs over  $\Delta t = \theta T$  time intervals. Large time FTLEs will be denoted as  $\mathcal{L}_i$ .

When oscillations are chaotic or hyperchaotic, computing large time FTLEs we deal with sums of nearly independent random values [45, 51]. It means that PDF of large time FTLEs is expected to be Gaussian, and the summation process can be treated as a diffusion process with linear growth of dispersion [45, 51]. When this is indeed the case, the diffusion of Lyapunov exponents is said to be normal. Otherwise it is anomalous. Below we will see that the considered system can demonstrate behaviors of both types.

#### 3.4.1. Distributions of large time FTLE

Figure 11 shows PDFs for the first large time FTLE computed at  $\theta = 256, 1024, \text{ and } 4096$ . The left column represents  $\mathcal{L}_1$  itself and the right one is for absolute values of deviations of  $\mathcal{L}_1$  from the mean value that is the mere global Lyapunov exponent,  $\langle \mathcal{L}_1 \rangle = \lambda_1$ . In the right column logarithmic scale is used on the vertical axis. Panels (a), (b), (c), and (d) in this figure correspond to the areas from A to D.



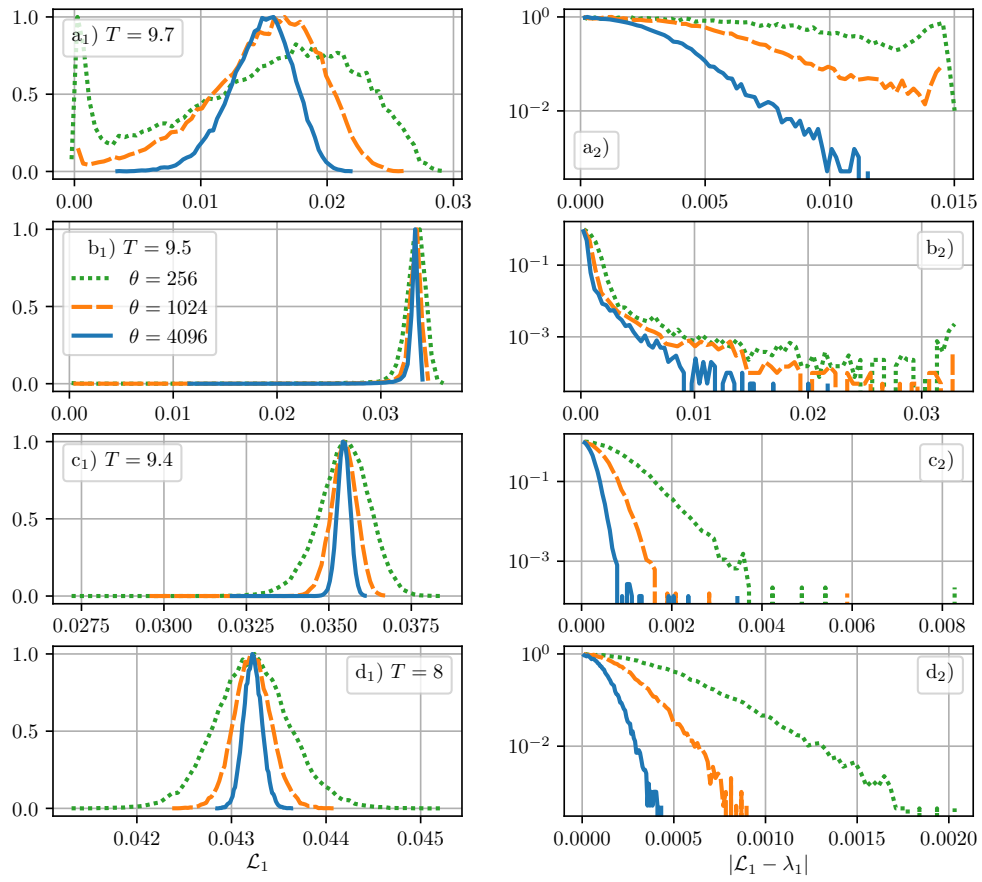


Figure 11: PDFs of large time FTLE  $\mathcal{L}_1$  computed on increasing time scales  $\theta = 256, 1024, \text{ and } 4096$ . Log scale is used for the vertical axes in the right column.

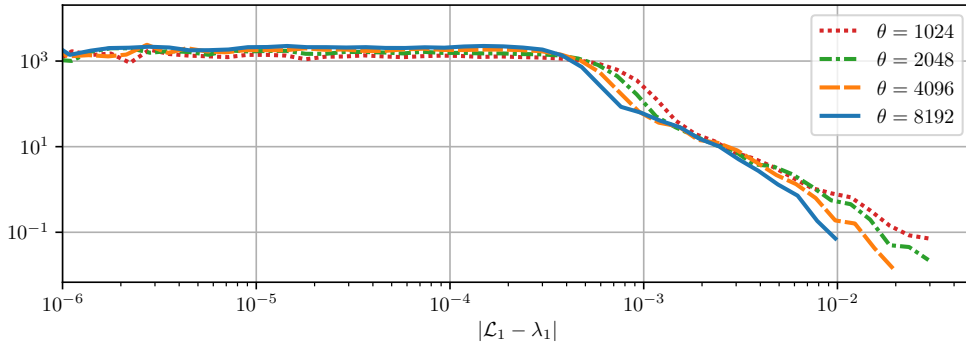


Figure 12: PDF for deviations of  $\mathcal{L}_1$  on increasing time scales for  $T = 9.5$ . Log-log scale is used. Observe power-law decay of tails. Estimated values of the exponent  $\alpha$  are  $(\theta, \alpha) = (1024, 2.24), (2048, 2.28), (4096, 3.16), (8192, 2.72)$

Figure 11(a) corresponds to the area A, where the system demonstrates intermittency. Distribution of laminar phases when the system stays near the origin obeys power law, see Fig. 7. It means that for any time length there is a nonzero probability to encounter this long laminar phase and hence nearly zero FTLE  $\mathcal{L}_1$  will be encountered regardless of  $\theta$ . As a result the corresponding PDF of  $\mathcal{L}_1$  always has a nonzero but asymptotically decaying peak at the origin. This is illustrated in Fig. 11(a<sub>1</sub>). One can see that this peak is very high at  $\theta = 256$ , and it is still visible at  $\theta = 1024$ . The left tail of the PDF at  $\theta = 4096$  does not reach the origin, but this is merely because the number of points accumulated to compute PDF was not enough to take into account very long laminar phases.

If we ignore the left end of the curve, the rest looks Gaussian. The main its feature, the exponentially decaying tails, is confirmed in Fig. 11(a<sub>2</sub>). One can see here that in the logarithmic scale on the vertical axis the tails of PDFs at  $\theta = 1024$  and  $\theta = 4096$  decay linearly that corresponds to the exponential law. This Gaussian form correlates with the uniform distribution of the one step FTLE  $\ell_1$  outside of the origin, see Fig. 5(a<sub>4</sub>).

In the area B there are two competing structures in the phase space: one is the fixed point at the origin and the other is a chaotic subset, see Fig. 5(b<sub>2</sub>). Their stability properties are strongly different. Wandering between them results in non Gaussian distributions of FTLEs. One can see in Fig. 11(b<sub>1</sub>) that regardless of the averaging time there is an essential tail spreading to the origin. This tail is also shown in Fig. 11(b<sub>2</sub>). One can see here that the deviations decay essentially slower than the exponent. To further characterize PDF in this case we re-plot it in Fig. 11(b<sub>2</sub>) in log-log scale, see Fig. 12. Linear decay of the tails indicate power law distribution, known as distribution with heavy tails. The exponents of this distribution  $\alpha$  are given in the figure caption. One can see that it approaches to 3 as  $\theta$  grows.

The PDFs in the areas C (non hyperbolic chaos) and D (hyperbolic chaos) demonstrate plain behaviors, typical for common chaotic dynamics. The curves are Gaussian, see Figs. 11(c<sub>1</sub>) and (d<sub>1</sub>) and their tails decay exponentially, see Figs. 11(c<sub>2</sub> and d<sub>2</sub>). Notice that this is observed regardless of the presence of the hyperbolicity. The Gaussian curves are formed because attractor does not contain competing subsets with strongly different stability properties.

### 3.4.2. Diffusion of Lyapunov exponents

Summation of FTLEs in the course of computation of Lyapunov exponents can be considered as a sort of random walking. If the summed values are random and independent, the variance of the sum is known to grow linearly in time. The coefficient of this growth, a diffusion coefficient, can be considered as one more characteristic quantifier of chaotic dynamics [45, 51]. This is the case for the most of chaotic systems no matter hyperbolic or not, and it is related with the Gaussian form of PDFs of FTLEs on large averaging times, see Figs. 11(c) and (d). But for non Gaussian distributions, like the one shown in Fig. 12(b), an anomalous diffusion occurs.

Let  $L_i(\theta)$  be a Lyapunov sum over  $\theta$  steps, i.e., this is a large time FTLE not divided by the computation

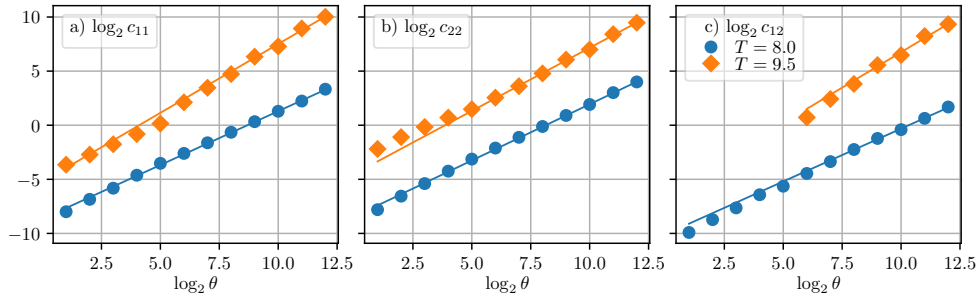


Figure 13: Power law approximation  $D\theta^\sigma$ , see Eqs. (10) and (11) for numerical values. Only four last points are used for computing the approximations.

time,  $\mathcal{L}_i = L_i(\theta)/T\theta$ , and let  $c_{ij} = \text{Covar}[L_i(\theta), L_j(\theta)]$  be a covariance of two Lyapunov sums. Trying to reveal anomalous diffusion we approximate the time dependence of the covariance via a power law

$$c_{ij} = D\theta^\sigma. \quad (9)$$

For a normal diffusion  $\sigma = 1$  and then  $D$  is a usual diffusion coefficient. Markers in Fig. 13 show  $c_{ij}$  for  $i, j = 1, 2$  as functions of  $\theta$  in log-log scale. Solid lines represent computed approximations. Line for  $c_{12}$  at  $T = 9.5$ , see Fig. 13(c), starts not from the origin, since  $c_{12}$  for smaller  $\theta$  are found to be negative. Observe that points are very good fitted to straight lines in the log-log scale. The computed approximations are as follows:

$$T = 8: \quad c_{11} = 0.0025 \theta^{1.00}, \quad c_{22} = 0.0028 \theta^{1.04}, \quad c_{12} = 0.00093 \theta^{0.98}, \quad (10)$$

$$T = 9.5: \quad c_{11} = 0.027 \theta^{1.27}, \quad c_{22} = 0.044 \theta^{1.17}, \quad c_{12} = 0.012 \theta^{1.31}. \quad (11)$$

We see that at  $T = 8$  corresponding to the area of hyperbolic chaos  $D \sigma \approx 1$ . It means that we have here the normal diffusion. The diffusion coefficients  $D$  are of the order  $10^{-3}$ . For a non Gaussian case  $T = 9.5$  in the area B, see Fig. 11(b),  $\sigma$  is definitely larger than 1. It means that here we have anomalous diffusion. But since  $\sigma$  is nevertheless close to 1, the comparison of  $D$  with the case at  $T = 8$  makes sense yet. We see that it is of order  $10^{-2}$ , i.e., one order higher. It indicates much higher amplitude of fluctuations of FTLEs at  $T = 9.5$ .

#### 4. Outline and discussion

In this paper we have considered a time delay system whose excitation parameter is periodically modulated so that it produces a sequence of oscillation pulses. Each new stage of excitation is seeded from one of the previous stages. Due to the specially tuned nonlinear mechanism, the seeding arrives with the doubled phase. Considering the system stroboscopically, i.e., reading its state after each excitation period, one observes hyperbolic chaotic dynamics. If the seeding is taken from the excitation stage before the last, the system operates as two coupled chaotic system working alternately. Varying the relation between delay time and excitation period we affect the coupling strength between these subsystems as well as the intensity of phase doubling mechanism responsible for the hyperbolicity. As a result, the transition from non-hyperbolic to hyperbolic hyperchaos occurs.

A decrease of the excitation period  $T$  at fixed delay time  $\tau$  corresponds to the weakening of coupling between the subsystems and the strengthening of the hyperbolicity mechanism. After regular oscillations, the hyperchaos appears almost immediately (an area with a single positive exponent was very narrow). Then, the following hyperchaotic regimes take place sequentially: (a) intermittency as an alternation of staying near a fixed point and chaotic bursts; (b) competition between the fixed point and chaotic subset

which appears near it; (c) plain hyperchaos without hyperbolicity after termination visiting neighborhoods of the fixed point; (d) transformation of chaos to hyperbolic form.

The competition in the regime (b) results in non-Gaussian distribution of large time FTLE with power law tails and power law growth of Lyapunov sum. This type of behavior related with wandering of trajectories near subsets with different numbers of expanding directions is called unstable dimension variability (UDV). Usually it is observed as a part of scenario of destruction of chaotic synchronization of two subsystems [24]. In our case we also can talk on two chaotic subsystems with rather non-trivial interaction. The UDV effect is observed for them as their coupling strength is decreased.

The transition to hyperbolic hyperchaos (d) is accompanied by vanishing of the embedded into the attractor non-hyperbolic chaotic subset, that we have detected using covariant Lyapunov vectors. The hyperbolic hyperchaos in turn is found to be of two types. The difference is due to the presence of low dimensional embedded hyperbolic chaotic subset. When it is visited by trajectories, the attractor gets more complicated structure with higher Kaplan-Yorke dimension, and after its vanish the system operates just as two weakly coupled identical hyperbolic chaotic subsystems.

*Declarations of interest: none*

## References

- [1] T. Kapitaniak, L. O. Chua, Hyperchaotic attractors of unidirectionally-coupled Chua's circuits, *International Journal of Bifurcation and Chaos* 04 (02) (1994) 477–482. doi:10.1142/S0218127494000356.
- [2] O. Rössler, An equation for hyperchaos, *Physics Letters A* 71 (2) (1979) 155–157. doi:10.1016/0375-9601(79)90150-6.
- [3] S. Nikolov, S. Clodong, Hyperchaos-chaos-hyperchaos transition in modified Rössler systems, *Chaos, Solitons & Fractals* 28 (1) (2006) 252–263. doi:10.1016/j.chaos.2005.05.031.
- [4] L. Kocarev, U. Parlitz, General approach for chaotic synchronization with applications to communication, *Phys. Rev. Lett.* 74 (1995) 5028–5031. doi:10.1103/PhysRevLett.74.5028.
- [5] J. H. Peng, E. J. Ding, M. Ding, W. Yang, Synchronizing hyperchaos with a scalar transmitted signal, *Phys. Rev. Lett.* 76 (1996) 904–907. doi:10.1103/PhysRevLett.76.904.
- [6] L. Yaowen, G. Guangming, Z. Hong, W. Yinghai, G. Liang, Synchronization of hyperchaotic harmonics in time-delay systems and its application to secure communication, *Phys. Rev. E* 62 (2000) 7898–7904. doi:10.1103/PhysRevE.62.7898.
- [7] J. Wang, W. Yu, J. Wang, Y. Zhao, J. Zhang, D. Jiang, A new six-dimensional hyperchaotic system and its secure communication circuit implementation, *International Journal of Circuit Theory and Applications* 47 (5) (2019) 702–717. doi:10.1002/cta.2617.
- [8] F. Sun, S. Liu, Z. Li, Z. Lü, A novel image encryption scheme based on spatial chaos map, *Chaos, Solitons & Fractals* 38 (3) (2008) 631–640. doi:10.1016/j.chaos.2008.01.028.
- [9] C. Zhu, A novel image encryption scheme based on improved hyperchaotic sequences, *Optics Communications* 285 (1) (2012) 29–37. doi:10.1016/j.optcom.2011.08.079.
- [10] Shujun Li, Xuan Zheng, Cryptanalysis of a chaotic image encryption method, in: 2002 IEEE International Symposium on Circuits and Systems. Proceedings (Cat. No.02CH37353), Vol. 2, 2002, pp. II–II. doi:10.1109/ISCAS.2002.1011451.
- [11] R. Rhouma, S. Belghith, Cryptanalysis of a new image encryption algorithm based on hyper-chaos, *Physics Letters A* 372 (38) (2008) 5973–5978. doi:10.1016/j.physleta.2008.07.057.
- [12] S. Torkamani, E. A. Butcher, M. D. Todd, G. Park, Hyperchaotic probe for damage identification using nonlinear prediction error, *Mechanical Systems and Signal Processing* 29 (2012) 457–473. doi:10.1016/j.ymsp.2011.12.019.
- [13] S. P. Kuznetsov, *Hyperbolic Chaos: A Physicist's View*, Higher Education Press: Beijing and Springer-Verlag: Berlin, Heidelberg, 2012.
- [14] S. Smale, Differentiable dynamical systems, *Bull. Amer. Math. Soc. (NS)* 73 (1967) 747–817.
- [15] D. V. Anosov (Ed.), *Dynamical Systems 9: Dynamical Systems with Hyperbolic Behaviour*, Vol. 9 of *Encyclopaedia Math. Sci.*, Berlin: Springer, 1995.
- [16] A. Katok, B. Hasselblatt, *Introduction to the Modern Theory of Dynamical Systems*, 1st Edition, Vol. 54 of *Encyclopedia of mathematics and its applications*, Cambridge University Press, 1995.
- [17] A. A. Andronov, L. S. Pontryagin, Structurally stable systems, in: *Dokl. Akad. Nauk SSSR*, Vol. 14, 1937, pp. 247–250.
- [18] A. A. Andronov, S. E. Khaikin, A. A. Vitt, *Theory of Oscillators*, Pergamon Press, 1966.
- [19] S. P. Kuznetsov, Dynamical chaos and uniformly hyperbolic attractors: from mathematics to physics, *Physics-Uspekhi* 54 (2) (2011) 119–144. doi:10.3367/ufne.0181.201102a.0121.
- [20] P. V. Kuptsov, S. P. Kuznetsov, Violation of hyperbolicity in a diffusive medium with local hyperbolic attractor, *Phys. Rev. E* 80 (2009) 016205. doi:10.1103/PhysRevE.80.016205.
- [21] P. V. Kuptsov, Violation of hyperbolicity via unstable dimension variability in a chain with local hyperbolic chaotic attractors, *Journal of Physics A: Mathematical and Theoretical* 46 (2013) 254016. doi:10.1088/1751-8113/46/25/254016.
- [22] E. J. Kostelich, I. Kan, C. Grebogi, E. Ott, J. A. Yorke, Unstable dimension variability: A source of nonhyperbolicity in chaotic systems, *Physica D: Nonlinear Phenomena* 109 (1) (1997) 81–90, proceedings of the Workshop on Physics and Dynamics between Chaos, Order, and Noise. doi:10.1016/S0167-2789(97)00161-9.

- [23] R. F. Pereira, S. E. de S. Pinto, R. L. Viana, S. R. Lopes, C. Grebogi, Periodic orbit analysis at the onset of the unstable dimension variability and at the blowout bifurcation, *Chaos: An Interdisciplinary Journal of Nonlinear Science* 17 (2) (2007) 023131. doi:10.1063/1.2748619.
- [24] T. Kapitaniak, Y. Maistrenko, S. Popovych, Chaos-hyperchaos transition, *Phys. Rev. E* 62 (2000) 1972–1976. doi:10.1103/PhysRevE.62.1972.
- [25] S. Yanchuk, T. Kapitaniak, Chaos-hyperchaos transition in coupled Rössler systems, *Physics Letters A* 290 (3) (2001) 139–144. doi:10.1016/S0375-9601(01)00651-X.
- [26] S. Yanchuk, T. Kapitaniak, Symmetry-increasing bifurcation as a predictor of a chaos-hyperchaos transition in coupled systems, *Phys. Rev. E* 64 (2001) 056235. doi:10.1103/PhysRevE.64.056235.
- [27] T. Vyhřidal, J. F. Lafay, R. Sipahi (Eds.), *Delay Systems: From Theory to Numerics and Applications*, Vol. 1, Springer Science & Business Media, 2013.
- [28] S. P. Kuznetsov, V. I. Ponomarenko, Realization of a strange attractor of the Smale-Williams type in a radiotechnical delay-feedback oscillator, *Tech. Phys. Lett.* 34 (9) (2008) 771–773. doi:10.1134/S1063785008090162.
- [29] S. P. Kuznetsov, A. Pikovsky, Attractor of Smale-Williams type in an autonomous time-delay system, Preprint nlin. arXiv:1011.5972 (2010). arXiv:1011.5972.
- [30] S. P. Kuznetsov, A. Pikovsky, Hyperbolic chaos in the phase dynamics of a q-switched oscillator with delayed nonlinear feedbacks, *EPL (Europhysics Letters)* 84 (1) (2008) 10013. doi:10.1209/0295-5075/84/10013.
- [31] S. V. Baranov, S. P. Kuznetsov, V. I. Ponomarenko, Chaos in the phase dynamics of Q-switched van der Pol oscillator with additional delayed-feedback loop, *Izvestiya VUZ. Applied Nonlinear Dynamics (Saratov)* 18 (1) (2010) 12–23, in Russian. doi:10.18500/0869-6632-2010-18-1-12-23.
- [32] A. S. Kuznetsov, S. P. Kuznetsov, Parametric generation of robust chaos with time-delayed feedback and modulated pump source, *Communications in Nonlinear Science and Numerical Simulation* 18 (3) (2013) 728–734. doi:10.1016/j.cnsns.2012.08.006.
- [33] D. S. Arzhanukhina, S. P. Kuznetsov, Robust chaos in autonomous time-delay system, *Izvestiya VUZ. Applied Nonlinear Dynamics (Saratov)* 22 (2) (2014) 36–49, in Russian. arXiv:arxiv:1404.4221, doi:10.18500/0869-6632-2014-22-2-36-49.
- [34] P. V. Kuptsov, S. P. Kuznetsov, Numerical test for hyperbolicity of chaotic dynamics in time-delay systems, *Phys. Rev. E* 94 (2016) 010201(R). doi:10.1103/PhysRevE.94.010201.
- [35] P. V. Kuptsov, S. P. Kuznetsov, Numerical test for hyperbolicity in chaotic systems with multiple time delays, *Communications in Nonlinear Science and Numerical Simulation* 56 (2018) 227–239. doi:10.1016/j.cnsns.2017.08.016.
- [36] P. V. Kuptsov, Fast numerical test of hyperbolic chaos, *Phys. Rev. E* 85 (2012) 015203. doi:10.1103/PhysRevE.85.015203.
- [37] S. V. Baranov, S. P. Kuznetsov, Hyperchaos in a system with delayed feedback loop based on Q-switched van der Pol oscillator, *Izvestiya VUZ. Applied Nonlinear Dynamics (Saratov)* 18 (4) (2010) 111–120, in Russian. doi:10.18500/0869-6632-2010-18-4-111-120.
- [38] F. Ginelli, P. Poggi, A. Turchi, H. Chaté, R. Livi, A. Politi, Characterizing dynamics with covariant lyapunov vectors, *Phys. Rev. Lett.* 99 (2007) 130601. doi:10.1103/PhysRevLett.99.130601.
- [39] C. L. Wolfe, R. M. Samelson, An efficient method for recovering lyapunov vectors from singular vectors, *Tellus A: Dynamic Meteorology and Oceanography* 59 (3) (2007) 355–366. doi:10.1111/j.1600-0870.2007.00234.x.
- [40] P. V. Kuptsov, U. Parlitz, Theory and computation of covariant Lyapunov vectors, *J. Nonlinear. Sci.* 22 (5) (2012) 727–762. doi:10.1007/s00332-012-9126-5.
- [41] A. Pikovsky, A. Politi, *Lyapunov Exponents: A Tool to Explore Complex Dynamics*, Cambridge University Press, 2016.
- [42] J. L. Kaplan, J. A. Yorke, Chaotic behavior of multidimensional difference equations, in: H.-O. Peitgen, H.-O. Walter (Eds.), *Functional differential equations and approximations of fixed points*, Vol. 730 of *Lecture Notes in Mathematics*, Springer, Berlin, 1979, p. 204. doi:10.1007/BFb0064319.
- [43] P. Grassberger, I. Procaccia, Measuring the strangeness of strange attractors, *Physica D: Nonlinear Phenomena* 9 (1) (1983) 189–208. doi:10.1016/0167-2789(83)90298-1.
- [44] P. V. Kuptsov, S. P. Kuznetsov, Lyapunov analysis of strange pseudohyperbolic attractors: angles between tangent subspaces, local volume expansion and contraction, *Regular and Chaotic Dynamics* 23 (7-8) (2018) 908–932. doi:10.1134/S1560354718070079.
- [45] P. V. Kuptsov, A. Politi, Large-deviation approach to space-time chaos, *Phys. Rev. Lett.* 107 (2011) 114101. doi:10.1103/PhysRevLett.107.114101.
- [46] R. L. Davidchack, Y.-C. Lai, Efficient algorithm for detecting unstable periodic orbits in chaotic systems, *Phys. Rev. E* 60 (1999) 6172–6175. doi:10.1103/PhysRevE.60.6172.
- [47] J. Crofts, R. Davidchack, Efficient detection of periodic orbits in chaotic systems by stabilizing transformations, *SIAM Journal on Scientific Computing* 28 (4) (2006) 1275–1288. doi:10.1137/050623401.
- [48] J. J. Crofts, R. L. Davidchack, On the use of stabilizing transformations for detecting unstable periodic orbits in high-dimensional flows, *Chaos: An Interdisciplinary Journal of Nonlinear Science* 19 (3) (2009) 033138. doi:10.1063/1.3222860.
- [49] J. B. Tenenbaum, V. d. Silva, J. C. Langford, A global geometric framework for nonlinear dimensionality reduction, *Science* 290 (5500) (2000) 2319–2323. doi:10.1126/science.290.5500.2319.
- [50] J. Alstott, E. Bullmore, D. Plenz, powerlaw: A python package for analysis of heavy-tailed distributions, *PLOS ONE* 9 (1) (2014) 1–11. doi:10.1371/journal.pone.0085777.
- [51] H. Fujisaka, Statistical dynamics generated by fluctuations of local Lyapunov exponents, *Progress of Theoretical Physics* 70 (5) (1983) 1264–1275. doi:10.1143/PTP.70.1264.